Title
MECHANICAL PROPERTIES OF BRITTLE MATRIX COMPOSITES

Authors
Stett, M.A.
Fulrath, R.M.

Publication Date
1969-06-01

Submitted to American Inst. of
Astronautics and Aeronautics

UCRL-18723
Preprint

MECHANICAL PROPERTIES OF BRITTLE MATRIX COMPOSITES

M. A. Stett and R. M. Fulrath

June 1969

AEC Contract No. W-7405-eng-48

LAWRENCE RADIATION LABORATORY
UNIVERSITY of CALIFORNIA BERKELEY

DISCLAIMER

MECHANICAL PROPERTIES OF BRITTLE MATRIX COMPOSITES

M. A. Stett* and R. M. Fulrath

Inorganic Materials Research Division, Lawrence Radiation Laboratory, and Department of Materials Science and Engineering, College of Engineering, University of California, Berkeley, California

June 1969

ABSTRACT

Systems composed of an inorganic glass matrix with metallic or inorganic crystal microspheres as the dispersed phase have been used as models for strength and elasticity studies. Parameters such as volume fraction of the dispersed phase, size and shape of the dispersed phase particles, thermal expansion mismatch between phases, and interfacial bonding between phases have been independently controlled. The strength and elasticity of this type composite system are discussed based on these parameters.

---

* Presently at Kaiser Aluminum and Chemical Corporation, Milpitas, Calif.

Supported by the United States Atomic Energy Commission under Contract W-7405-eng-48.

At the time this work was done the writers were, respectively, research assistant and professor of ceramic engineering, Department of Materials Science and Engineering, College of Engineering, and Inorganic Materials Research Division, Lawrence Radiation Laboratory, University of California, Berkeley.

I. INTRODUCTION

In order to predict the mechanical behavior and to develop new brittle matrix composite materials, a quantitative understanding of the basic mechanisms of failure of these composite materials is necessary. The properties of composite materials will depend upon the properties of the individual components, their distribution, and their interaction. Thermal expansion differences and varied elastic properties result in internal stresses and stress inhomogeneities under applied load, respectively. Chemical bonding between the phases further complicates the situation. Microstructural control in the fabrication of the composites may introduce the factor of the distribution of the two phases.

In this discussion we examine the progress that has been made in the understanding of these systems. The elastic properties and strength of a brittle glass matrix containing dispersions of controlled volume fraction, particle shape, particle size, and particle character were investigated. Glass is an ideal brittle material and by controlling the composition of a glass, a wide range of thermal expansion coefficients may be achieved. Further, the viscosity characteristics of glass allow relatively low temperature fabrication of a theoretically dense composite system by vacuum hot-pressing. Strengths of systems with and without internal stresses were investigated considering particle size, particle volume fraction, stress concentration effects, and interphase bonding.

II. POROUS SYSTEMS

Effect of Porosity on Elastic Modulus

The evolution of CO_2 and H_2O from Na_2CO_3 and boric acid vapor during the formation of D glass (16% Na_2O, 14% B_2O_3, and 70% SiO_2) provided a method for the formation of a measurable amount of spherical porosity.[1] The relative amount of bubbles in the melt was an inverse function of the length of time the melt was held at temperature. Figure 1 shows a photomicrograph of a specimen containing 1.62 vol. % porosity. The picture was made by focusing below the glass surface and because of the relatively high depth of field anomalously higher volume fractions are observed. The volume fraction of porosity that can be obtained by this method was limited to about 2.5 vol. %. Young's modulus and shear modulus were determined by a flexural and torsional resonance technique,[2] yielding two values of Young's modulus and one value of shear modulus for each specimen. A set of precompiled tables was used to calculate Young's modulus from the measured resonance frequency.[3] The shear modulus was calculated using the technique given by Spinner and Tefft.[2] True densities were measured using a pycnometer technique and bulk densities from weights and dimensions. The index of refraction was used as a check on glass composition.

The experimental results were fitted by a least squares technique to the expressions

$$E = E_o (- \alpha_E P) \qquad (1)$$

$$G = G_o (1 - \alpha_G P)$$

where E is the Young's modulus, G is the shear modulus, P is the volume fraction porosity, the subscript o refers to the nonporous material, and α_E and α_G are constants. These results are shown in Fig. 2. Experimental values for α_E and α_G compared very well with theoretical values calculated from solutions for the effect of spherical porosity on shear modulus and bulk modulus.

Micromechanical Stress Concentrations

Under mechanical loading, differences in elastic properties of individual components can lead to stress concentrations. Theoretical solutions exist for stress concentrations associated with elastic inhomogeneities of various shapes in an infinite matrix. Since glass fracture is usually nucleated at the specimen surface and because of the high stress gradients in the strength test, Goodier's solutions for a circular inclusion in a flat plate[4] were used. Figure 3 describes the polar coordinate system used to describe the stress.

Using 331[1] and 0 kbars for the shear moduli of D glass and porosity, respectively, and 0.197[1] for Poisson's ratio of the glass, the following stress concentrations were calculated for small volume fractions and uniaxial loading

$$\sigma_r = 2T\left[-\frac{a^2}{4r^2} + \left(\frac{3a^4}{4r^4} - \frac{a^2}{r^2}\right)\cos 2\theta\right] + T\cos\theta \qquad (2)$$

$$\sigma_t = 2T\left[\frac{a^2}{4r^2} - \frac{3a^4}{4r^4}\cos 2\theta\right] + T\sin\theta \qquad (3)$$

and for biaxial loading

$$\sigma_r = 4T\left[-\frac{a^2}{4r^2}\right] + T \qquad (4)$$

$$\sigma_t = 4T\left[\frac{a^2}{4r^2}\right] + T \tag{5}$$

where T is the stress applied to the composite and the other terms are defined in Fig. 3. Under a tensile load (T positive), tensile stresses greater than the applied stress occur for Eqs. (3) and (5) and if stress concentrations affect tensile strength, the tangential component will lead to fracture. It can also be seen that maximum stress concentration will occur at the interface (r = a) and will be independent of angular orientation under biaxial loading. Maximum tangential stresses are found to be 3T and 2T for uniaxial and biaxial stress, respectively. The hypothesis has been presented that the effect of micromechanical stress concentrations on the strength of a brittle material depends on the size of the Griffith flaw relative to the region over which the stress concentration acts. The effect of porosity on strength can be divided into three regions.[5] In region I the pore size is larger than the flaw size and the flaw lies entirely in material stressed to the maximum stress concentration. Engineering structures with drilled holes or grooves in otherwise pore-free materials fall in this region where the introduction of even a single pore instantaneously decreases the strength of the non-porous material. The decrease in strength will correspond to the maximum stress concentration factor. This can be seen in Fig. 4. For region III the pore is considerably smaller than the Griffith flaw which will be completely unaffected by the stress concentrations near the pores. A decrease in strength should be observed, but without the precipitous decrease as in region I. In region II the flaw size is of the order of the pore size and only part of the flaw lies within the stress concentration.

Results of tests for both uniaxial and biaxial loading can be seen in Figs. 5-6.[6] In a previous investigation[7] it was suggested that, neglecting stress concentrations, the strength of the composite should follow the relation

$$S = So\ (1 - \phi)^{-1/2} \qquad (6)$$

where S and So are the strength of the composite and matrix, respectively, and ϕ is the volume fraction second phase. The experimental results shown in Fig. 5 and Fig. 6 suggest that a stress concentration factor, K, should be introduced.

$$S = \frac{So}{K}\ (1 - \phi)^{1/2} \qquad (7)$$

Figure 7 is a diagram of stress contours in the two cases considered. The fact that there is an area of higher stress concentration than 2T in the uniaxial case can account for the lower observed strengths. Region III seems to be approached more rapidly in the biaxial case than in the uniaxial case.

III. NONPOROUS SYSTEMS

Al_2O_3 Dispersant

Theoretical expressions[8-10] for the elastic moduli of the two-phase systems were compared using the Al_2O_3-D glass system.[11] The procedures were the same as those used in the porosity-glass system. D glass and Al_2O_3 have nearly identical coefficients of thermal expansion and Al_2O_3 has an elastic modulus considerably higher than that of D glass.

Experimental and theoretical results can be seen in Fig. 8. The experimental results agree well with Hashin and Shtrikman's lower bound for arbitrary phase geometry which coincides with Hashin's approximate expression for spherical phase geometry.

Using 331[1] and 1635[12] kbars for the shear moduli of D glass and alumina, respectively, and 0.197[1] and 0.257[12] for Poisson's ratio for D glass and alumina, respectively, the stress concentrations in the glass matrix under uniaxial loading for small volume fractions were

$$\sigma_r = 2T\left[0.107\frac{a^2}{r^2} + \left(-0.267\frac{a^4}{r^4} + 0.356\frac{a^2}{r^2}\right)\cos 2\theta\right] + T\cos\theta \quad (8)$$

$$\sigma_t = 2T\left[-0.107\frac{a^2}{r^2} + 0.267\frac{a^4}{r^4}\cos 2\theta\right] + T\sin\theta \quad (9)$$

under biaxial loading were

$$\sigma_r = 4T\left[0.107\frac{a^2}{r^2}\right] + T \quad (10)$$

$$\sigma_t = 4T\left[-0.107\frac{a^2}{r^2}\right] + T \quad (11)$$

where T is the stress applied to the composite and the other terms are defined in Fig. 3. Under conditions of tensile load, Eqs. (8) and (10) yield concentrations greater than one and failure will be due to these radial stresses. The value will be 1.39T under uniaxial load and 1.43T under biaxial load. Experimental results are shown in Fig. 9 and can be interpreted in a manner similar to the porosity-glass system. The biaxial strength value can be described quite accurately using Eq. (7).

The uniaxial strength results do not show a precipitous decline in strength on addition of the alumina phase.

For a flat plate containing an elliptical flaw, the Griffith expression for the macroscopic strength is

$$S_o = \left(\frac{4\gamma E}{\pi a} \right)^{1/2} \tag{12}$$

where γ is the surface energy, E is Young's modulus of elasticity, and a is the flaw size. A fracture theory has been proposed based on the limitation of flaw size by dispersions in a brittle matrix.[13] The result of limiting the flaw size will be a strength increase. Experimental results verifying this hypothesis are given in Fig. 10. In Area I the average distance between particles is greater than the flaw size and Eq. (6) is applicable. At higher volume fractions (Area II) the flaw size will be restricted to the average mean free path between particles. An expression for the mean free path, d, between spherical particles of uniform radius, R, distributed statistically throughout a matrix was provided by Fullman[14] as

$$d = \frac{4R\ (1-\phi)}{3\phi} \tag{13}$$

Substituting Eq. (13) into Eq. (12) we find the strength in Area II to be

$$S = \left(\frac{3\gamma E\ \phi}{\pi R\ (1-\phi)} \right)^{1/2} \tag{14}$$

This limitation of flaw size by the dispersed phase can be seen in Fig. 11. The discontinuity in Fig. 10 provides a measure of the original flaw size and the extension of the curve in Area II should pass through the origin.

The slope of the curve in Area II can be used to calculate the dynamic surface energy.

Two Particle Sizes

In order to obtain smaller mean free paths and to extend the data in Fig. 10, composites were made with a tungsten dispersant of more than one particle size.[15] Due to the inability to fabricate dense composites, mean free paths were limited to about 15μ with only one particle size. Using two particles in the W-Ny glass (65% SiO_2, 8.5% Na_2O, 26.5% B_2O_3) system it was possible to extend the mean free path limitation (Fig. 12) and with a 3-13μ particle size distribution a mean free path limitation of 6μ was obtained. A representative microstructure in this system is shown in Fig. 13. With two particle sizes, the mean free path was determined by a statistical technique.[16] The average mean free path, λ, was determined from the relation

$$\lambda = \frac{1-V_v}{N_L} \qquad (15)$$

where V_v is the volume fraction of the dispersed phase and N_L is the average number of particles intersected by a unit length of line. This value was used for "a" in Eq. (12) in order to determine strengths.

IV. BONDED SYSTEMS

Strengthening

Where no interphase bonding occurs, strengthening can be achieved through the mechanical formation of an interface between dispersant and matrix. By the chemical formation of that interface, an even greater strengthening can be obtained. Nason[17] attempted to examine the effect of an interfacial bond in the strengthing of glass matrix-dispersed metal systems. Composites fabricated from tungsten and a glass of lower thermal expansion showed an anomalous strengthening (Fig. 14). Pressure wetting experiments showed bonding (Fig. 15) between the two and not between nickel and another glass with a thermal expansion less than nickel. In the case of the nickel, weakening was noticed as would be expected for induced porosity and later verified by Bertolotti and Fulrath (Figs. 5-6). With small particle sizes, Bertolotti and Fulrath also observed an anomalous strengthening and proposed that adsorbed water on the surface of the glass powder used in fabricating the composite caused oxidation of the nickel surface and resulted in a bond between the oxidized nickel and the glass. Nickel microspheres that were pre-oxidized were hot-pressed with a glass of lower thermal expansion (D glass) and it was shown that the bond did, indeed, prevent the shrinkage of the nickel away from the glass and provide strengthening in a normally porous system (Fig. 16). In a system where the thermal expansion of the glass is greater than that of the nickel and strengthening would be expected, even greater strengthening was observed (Fig. 17) when an interfacial bond was present. The dispersed phase should produce approximately 20% strengthening by flaw limitation in this case. The presence of the bond introduced another 30% strengthening. The mechanism of this extra strengthening is presently under investigation.

Fracture Behavior

Not only will the strength be affected by the presence of an interfacial bond, but the fracture behavior will also be altered. In a nonbonded system the fracture will propagate directly to and around a dispersed sphere because of stress concentrations around a spherical cavity (Fig. 18). During the hot-pressing of the oxidized nickel-D glass composite, the interfacial bond is formed by the migration of nickel oxide into the glass until the glass is saturated with nickel oxide near the sphere. Because of the thermal expansion difference between this saturated glass, the nickel, and the matrix glass, a radial tensile stress is developed. To attempt to relieve this tension, a fracture will propagate around the sphere (Fig. 19) at a finite distance in the glass phase. This alteration of fracture behavior is presently being investigated for other systems.

V. SUMMARY

Strengthening of brittle matrix composite materials can be achieved through the limitation of the size of existing Griffith flaws. In porous systems the relative size of the Griffith flaws as compared to the average mean free path determines the effect of the porosity on strength. Under mechanical loading, the stress concentrations that arise from differences in elastic properties affect the composite strength. The existence of a bond between the two phases increases the strength markedly and alters the fracture behavior.

ACKNOWLEDGMENT

The scanning electron microscope used was operated within the Electronics Research Laboratory, University of California; it was purchased under Grant No. GB-6428 from the National Science Foundation and is operated under Grant No. GM 15536 from the National Institute of Health. This work was done under the auspices of the United States Atomic Energy Commission.

REFERENCES

1) Hasselman, D. P. H. and Fulrath, R. M., "Effect of Small Fraction of Spherical Porosity on Elastic Moduli of Glass," J. Am. Ceram. Soc. Vol. 47, No. 1, 1964, pp. 52-53.

2) Spinner, S. and Tefft, W. E., "Method for Determining Mechanical Resonance Frequencies and for Calculating Elastic Moduli from These Frequencies," Am. Soc. Testing Mater. Proc., 61, 1961, pp. 1221-1238; Ceram. Abstr., Oct. 1962, p. 248g.

3) Hasselman, D. P. H., "Tables for Computation of Shear Modulus and Young's Modulus of Elasticity from Resonant Frequencies of Rectangular Prisms," The Carborundum Company, Niagara Falls, New York, 1962, 195 pp.

4) Goodier, J. M., "Concentration of Stress Around Spherical and Cylindrical Inclusions and Flaws," J. Appl. Mech., Vol. 1, No. 1, 1933, pp. 39-44.

5) Hasselman, D. P. H. and Fulrath, R. M., "Micromechanical Stress Concentrations in Two-Phase Brittle-Matrix Composites," J. Am. Ceram. Soc., Vol. 50, No. 8, 1967, pp. 399-404.

6) Bertolotti, R. L. and Fulrath, R. M., "Effect of Micromechanical Stress Concentrations on Strength of Porous Glass," J. Am. Ceram. Soc., Vol. 50, No. 11, 1967, pp. 558-562.

7) Hasselman, D. P. H., and Fulrath, R. M., "Proposed Fracture Theory of a Dispersion-Strengthened Glass Matrix," J. Am. Ceram. Soc. Vol. 49, No. 2, 1966, pp. 68-72.

8) Paul, B., "Prediction of Elastic Constants of Multiphase Materials," Trans. AIME, Vol. 218, No. 1, 1960, pp. 36-41.

9) Hashin, Z., "Elastic Moduli of Heterogeneous Materials," J. Appl. Mech., Vol. 29, No. 1, 1962, pp. 143-50.

10) Hashin, Z. and Shtrikman, S., "A Variational Approach to the Theory of the Elastic Behavior of Multiphase Materials," J. Mech. Phys. Solids, Vol. 11, No. 2, 1963, pp. 127-140.

11) Hasselman, D. P. H., and Fulrath, R. M., "Effect of Alumina Dispersions on Young's Modulus of a Glass," J. Am. Ceram. Soc., Vol. 48, No. 4, 1965, pp. 218-219.

12) Spriggs, R. M. and Brisette, L. A., "Expressions for Shear Modulus and Poisson's Ratio of Porous Refractory Oxides," J. Am. Ceram. Soc., Vol. 45, No. 4, 1962, pp. 198-199.

13) Hasselman, D. P. H. and Fulrath, R. M., "Proposed Fracture Theory of a Dispersion-Strengthened Glass Matrix," J. Am. Ceram. Soc., Vol. 49, No. 2, 1966, pp. 68-72.

14) Fullman, R. L., "Measurement of Particle Sizes in Opaque Bodies," Trans. AIME, Vol. 197, No. 3, 1953, pp. 447-452.

15) Nivas, Y., "Limitation of Griffith Flaws in Glass Matrix Composites," Report UCRL-18586, Nov. 1968, Lawrence Radiation Laboratory, University of California, Berkeley.

16) Underwood, E. E., Colcord, A. R. and Waugh, R. C., "Quantitative Relationships for Random Microstructures," pp. 25-52 in Ceramic Microstructures: Their Analysis, Significance and Production, Edited by R. M. Fulrath and J. A. Pask, John Wiley & Sons, Inc., New York, 1968.

17) Nason, D. O., "Effect of Interfacial Bonding on Strength of a Model Two Phase System," Report UCRL-11011, Sept. 1963, Lawrence Radiation Laboratory, University of California, Berkeley.

18) Stett, M. A. and Fulrath, R. M., "Strengthening by Chemical Bonding in a Brittle Matrix Composite," J. Am. Ceram. Soc., Vol. 51, No. 10, 1968, pp. 599-600.

FIGURE CAPTIONS

Figure 1. Photomicrograph of sodium borosilicate glass specimen containing 1.62% porosity

Figure 2. Young's modulus, shear modulus, and index of refraction of sodium borosilicate glass as a function of pore content

Figure 3. Polar-coordinate system for description of stress concentrations

Figure 4. Proposed relative effect of spherical porosity on uniaxial tensile strength. I. Flaw size << pore size; II. Flaw size ≃ pore size; and III. Flaw size >> pore size

Figure 5. Uniaxial tensile strength of sodium borosilicate glass containing spherical pores

Figure 6. Biaxial tensile strength of sodium borosilicate glass containing spherical pores

Figure 7. Approximate tangential tensile stress concentration around a flat cylindrical pore under uniaxial and biaxial loading

Figure 8. Experimental and theoretical results for Young's modulus of sodium borosilicate glass as a function of the volume content of alumina particles

Figure 9. Uniaxial and biaxial strength of sodium borosilicate glass containing 60μ diameter alumina spheres

Figure 10. Experimental data for uniaxial strength of sodium borosilicate glass containing spherical alumina particles as a function of the reciprocal square root of the mean free path

Figure 11. Griffith cracks in polished surface of glass matrix containing (a) 0, (b) 10.9, and (c) 42.3 vol. % 15μ diameter spherical alumina

Figure 12. Experimental data for the strength of Ny glass and tungsten composites plotted as a function of reciprocal square root of measured mean free path

Figure 13. Photomicrograph of Ny glass and tungsten composite containing 63.2 vol. % tungsten spheres of sizes 70 and 10μ (72% coarse and 28% fine)

Figure 14. Rupture moduli of N4 glass and tungsten composites as a function of volume fraction tungsten

Figure 15. Photomacrographs from the pressure-wetting studies of the metal discs at the parted interfaces (1.9X) (a) nickel disc before (top) and after (b) tungsten disc before (top) and after

Figure 16. Strength of D glass and oxidized nickel composites as a function of weight gain during oxidation

Figure 17. Strength of 8 glass and oxidized nickel composites as a function of weight gain during oxidation

Figure 18. Scanning electron microscope photograph of fracture surface of non-bonded D glass and nickel composite

Figure 19. Scanning electron microscope photograph of fracture surface of bonded D glass and oxidized nickel composite

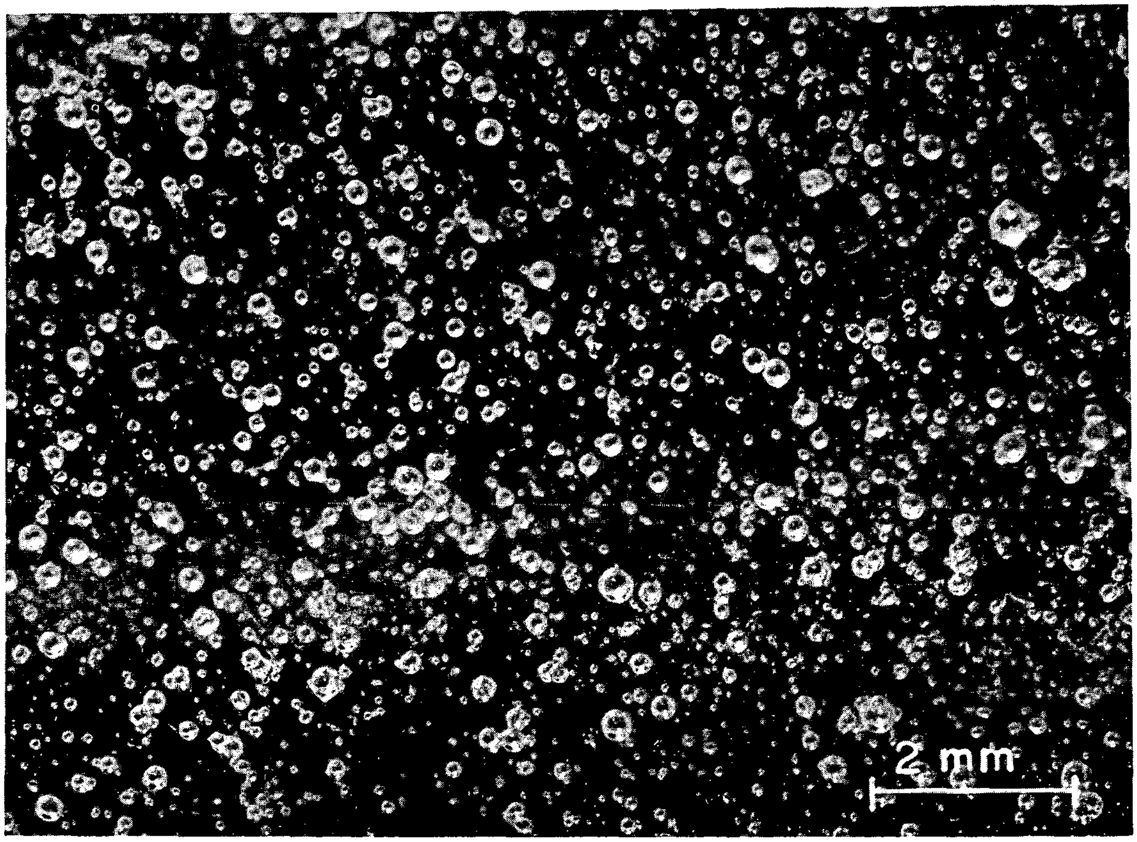

IM 1826

Fig. 1

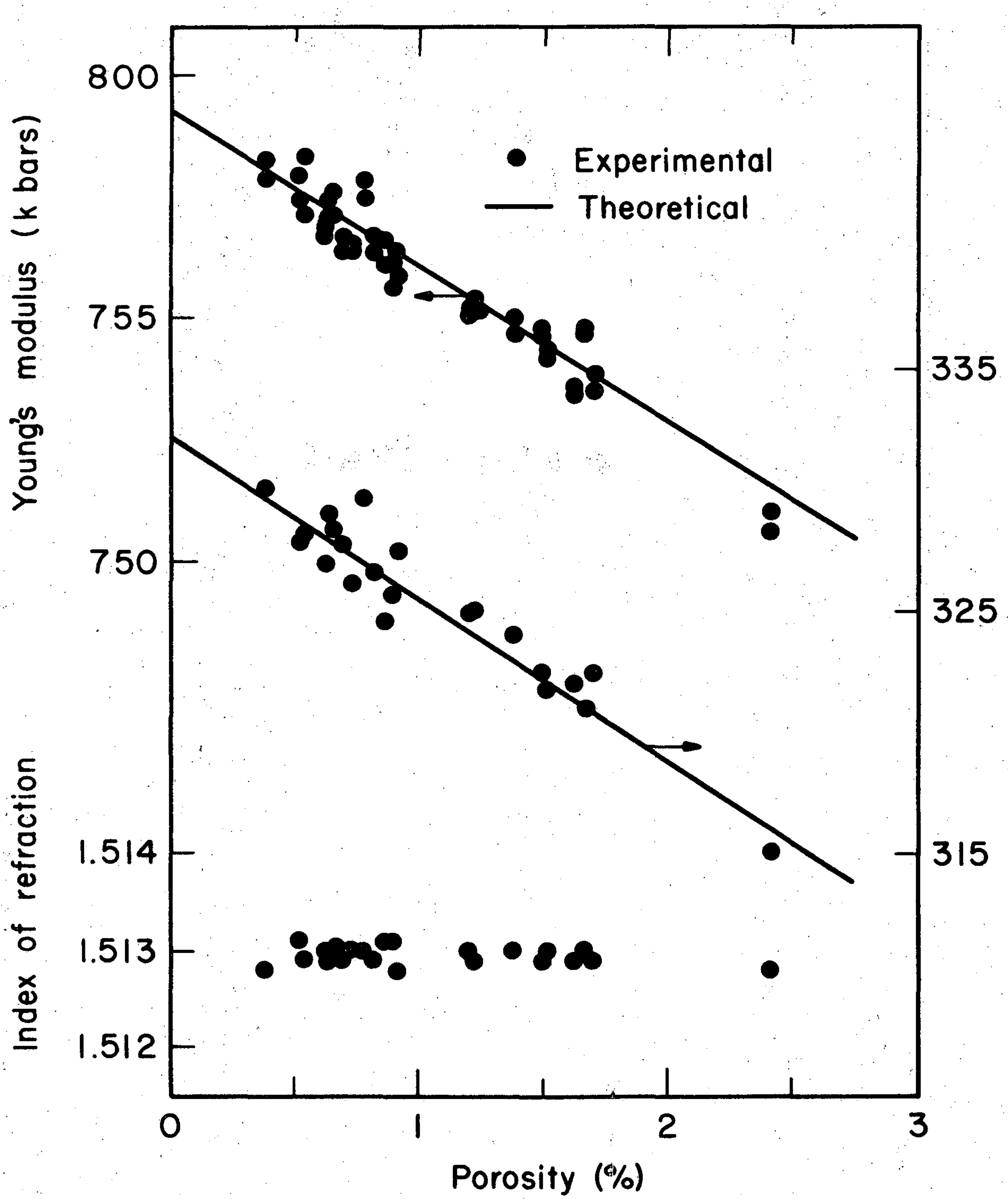

MU-32031

Fig. 2

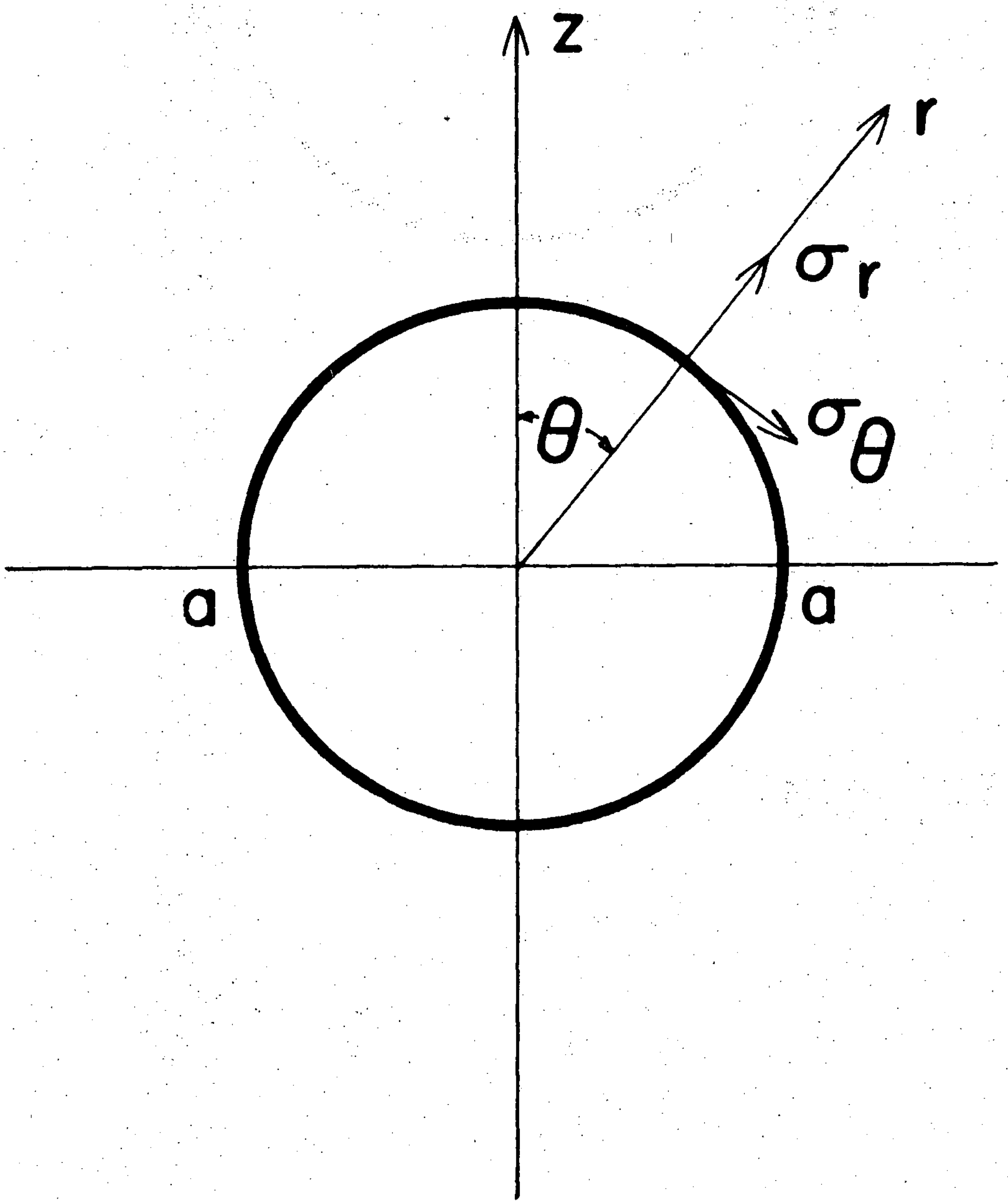

MUB-7874

Fig. 3

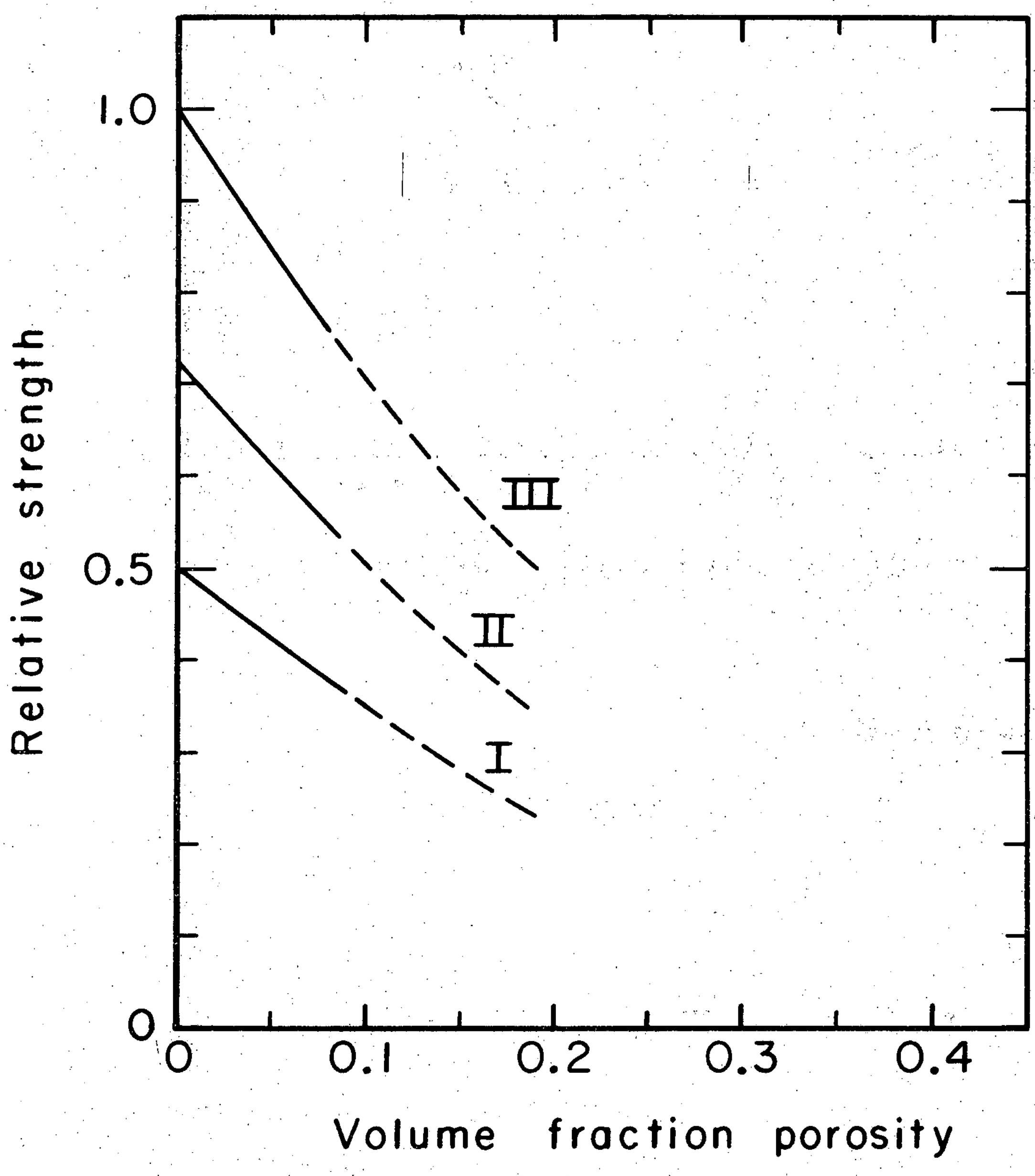

MUB-8103

Fig. 4.

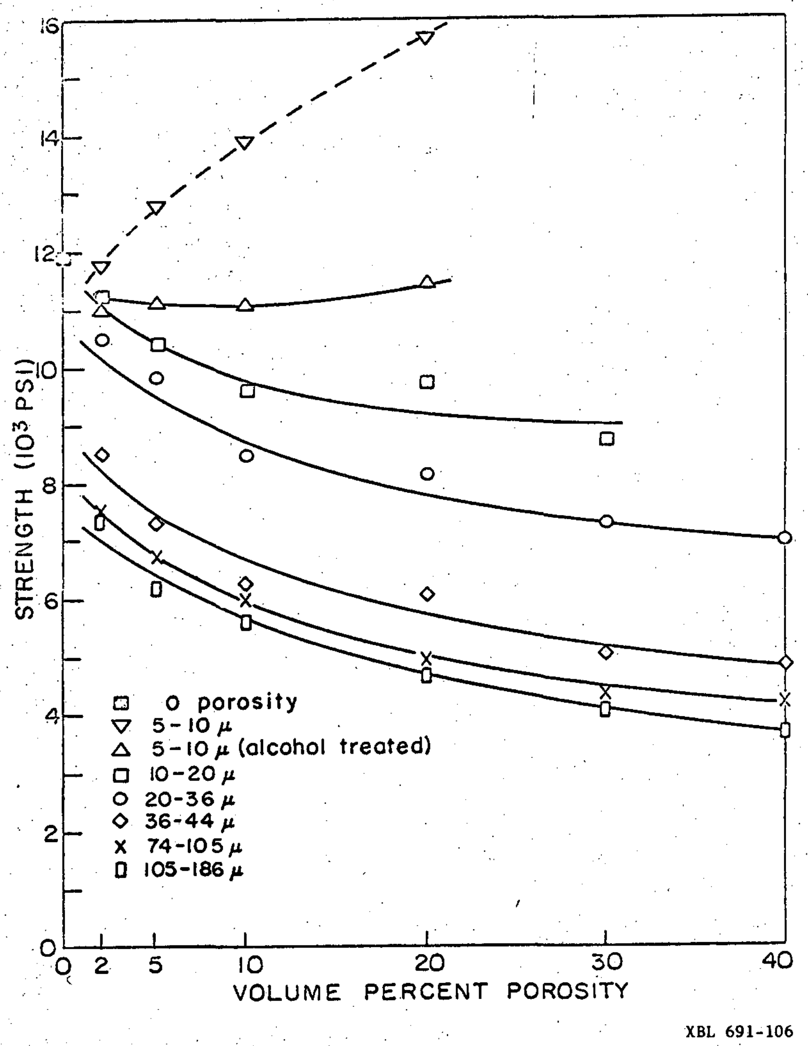
STRENGTH (10^3 PSI)
VOLUME PERCENT POROSITY
0 porosity
5-10 μ
5-10 μ (alcohol treated)
10-20 μ
20-36 μ
36-44 μ
74-105 μ
105-186 μ
XBL 691-106

Fig. 5.

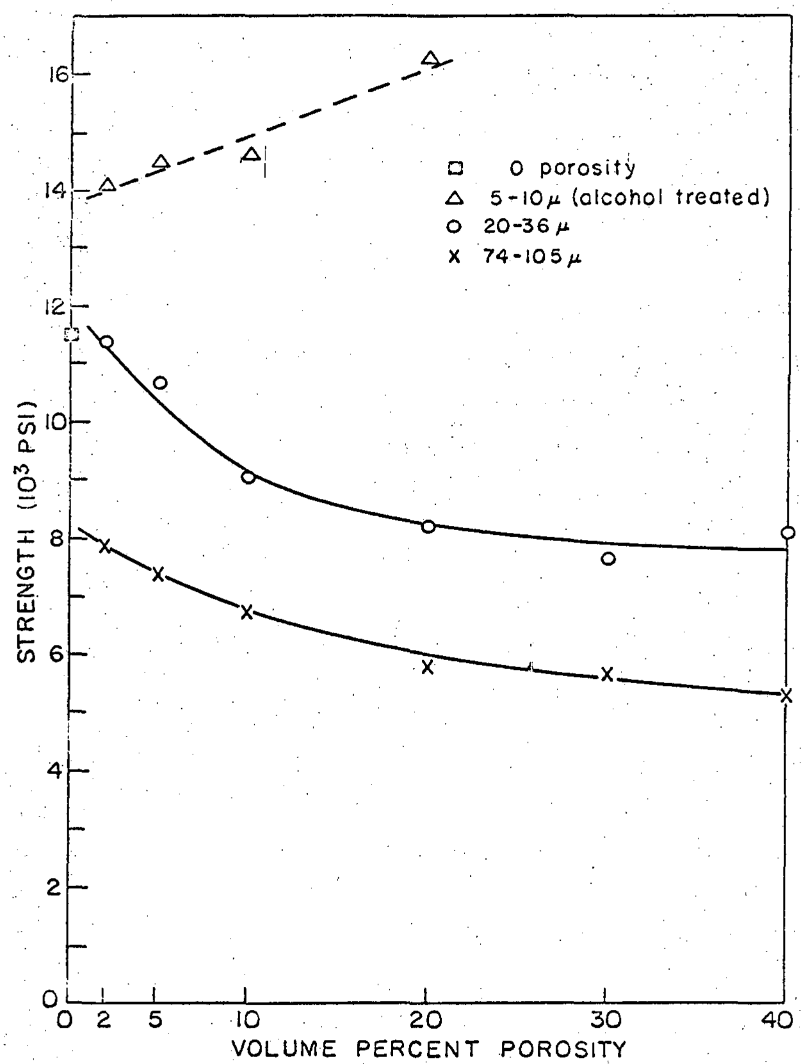

XBL 691-107

Fig. 6

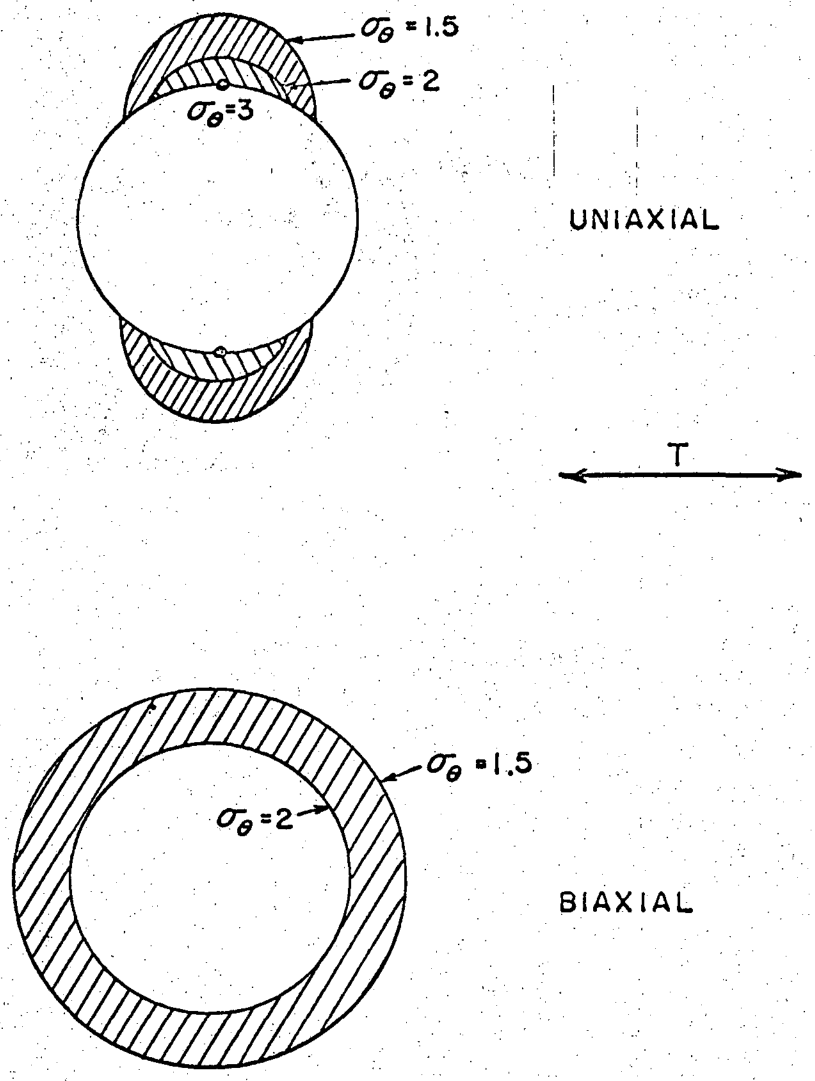

XBL 691-108

Fig. 7

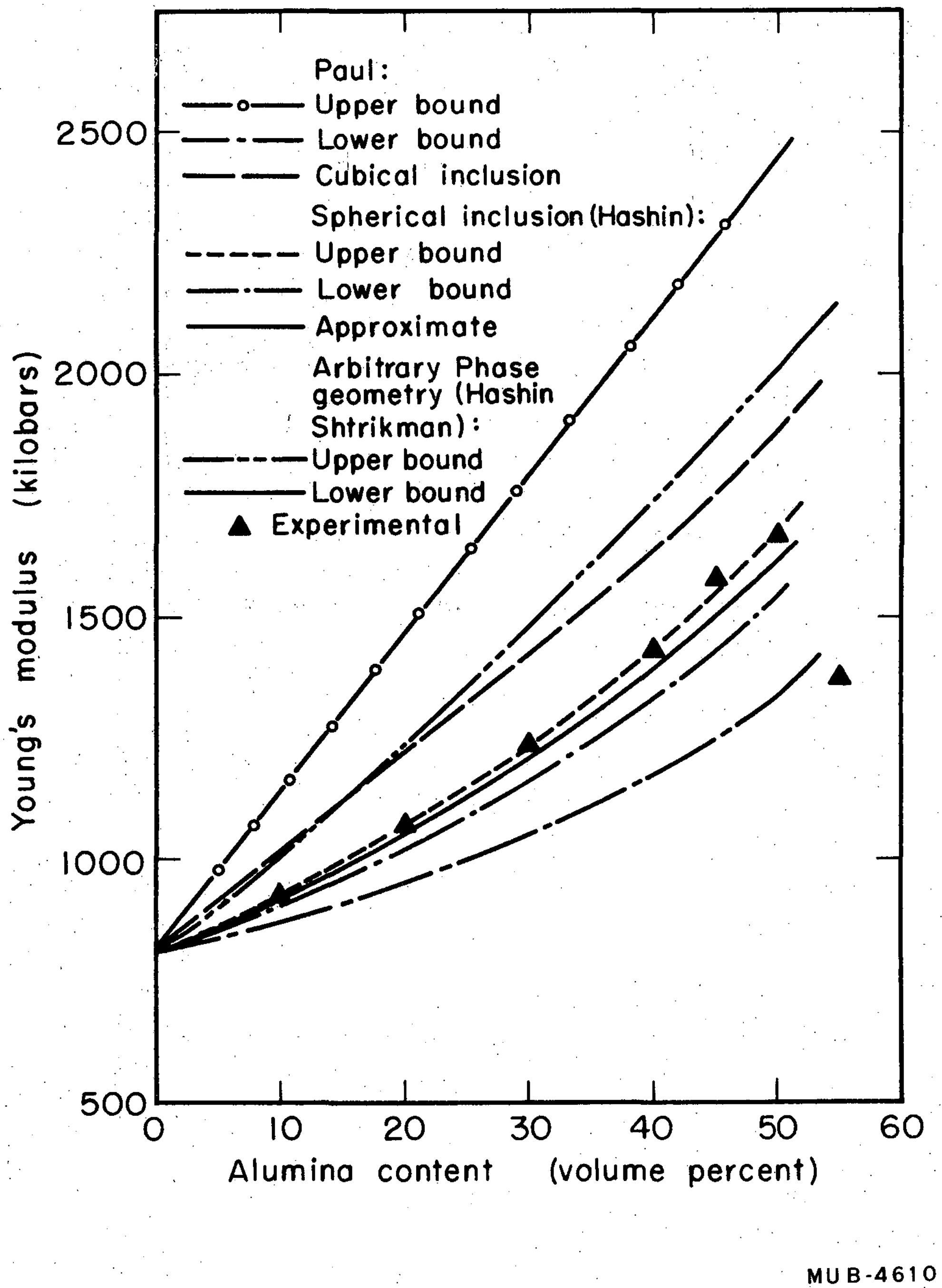
Paul:
Upper bound
Lower bound
Cubical inclusion
Spherical inclusion (Hashin):
Upper bound
Lower bound
Approximate
Arbitrary Phase geometry (Hashin Shtrikman):
Upper bound
Lower bound
Experimental
Young's modulus (kilobars)
2500
2000
1500
1000
500
0
10
20
30
40
50
60
Alumina content (volume percent)
MUB-4610

Fig. 8

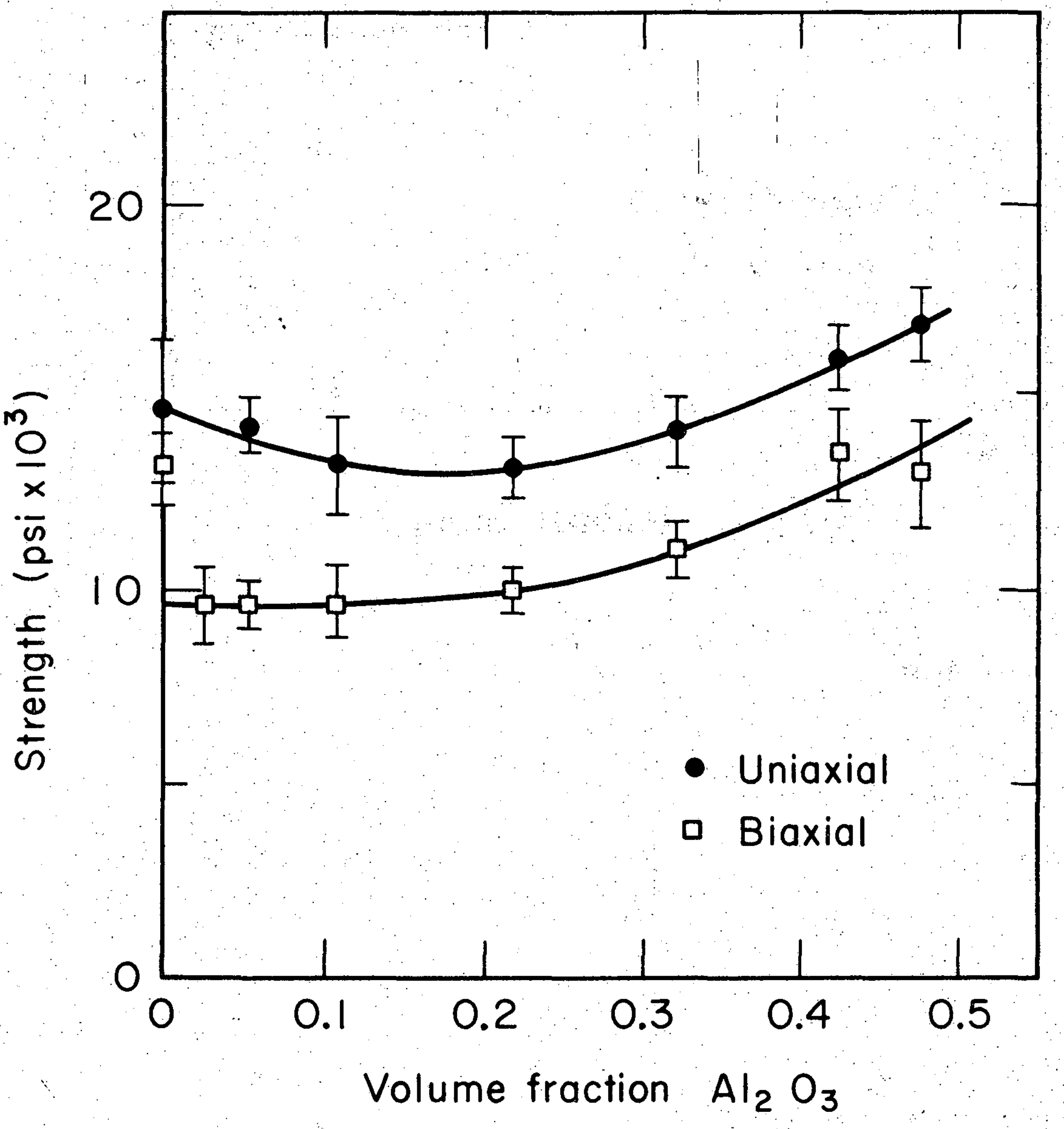

MUB-7856

Fig. 9

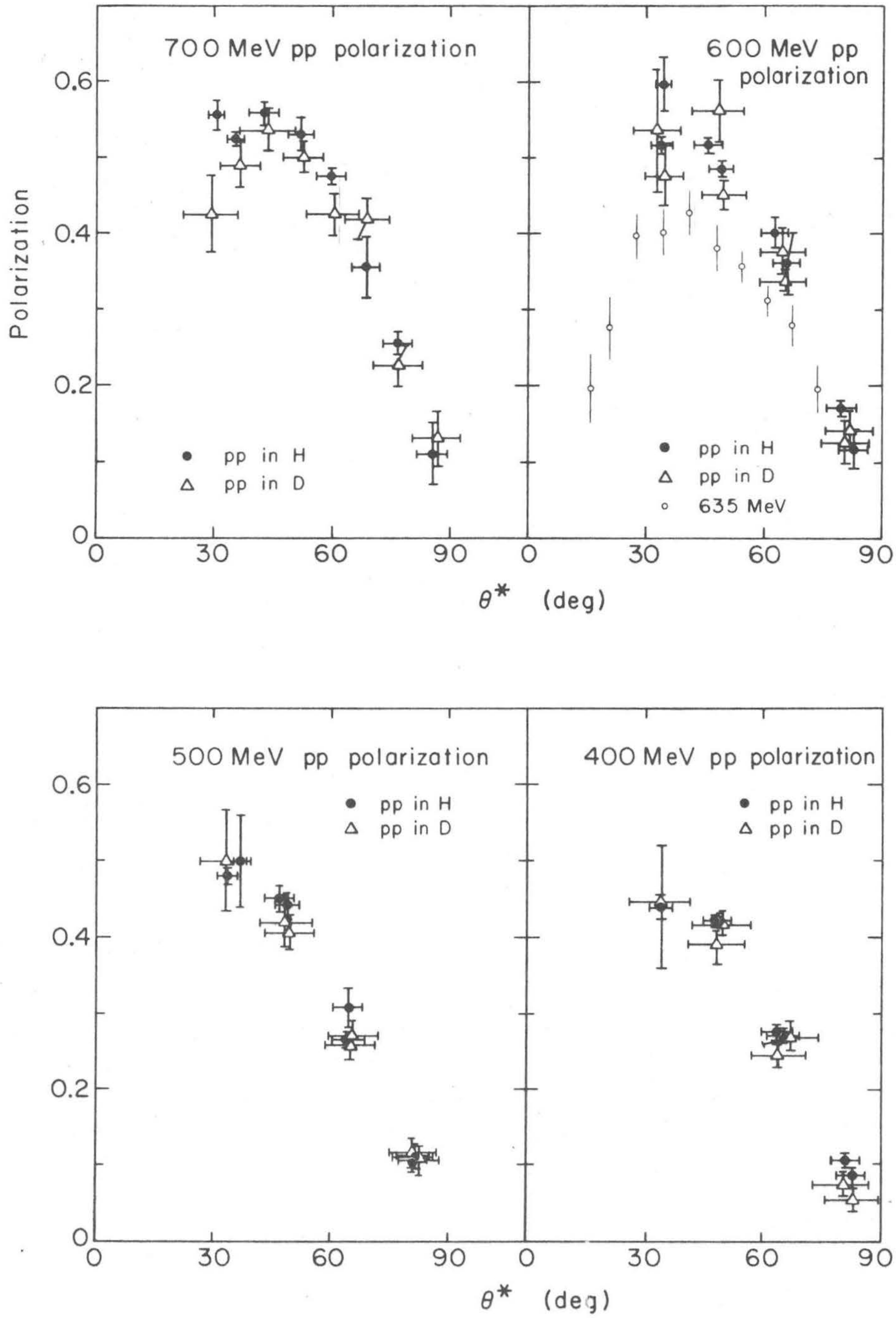

MUB-7611

Fig. 10

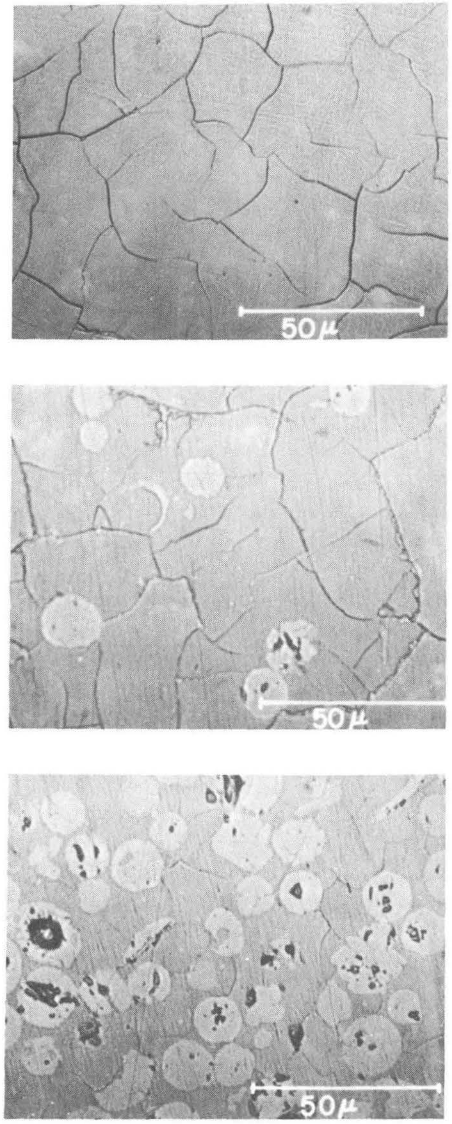

(a)

(b)

(c)

IM 1926

Fig. 11

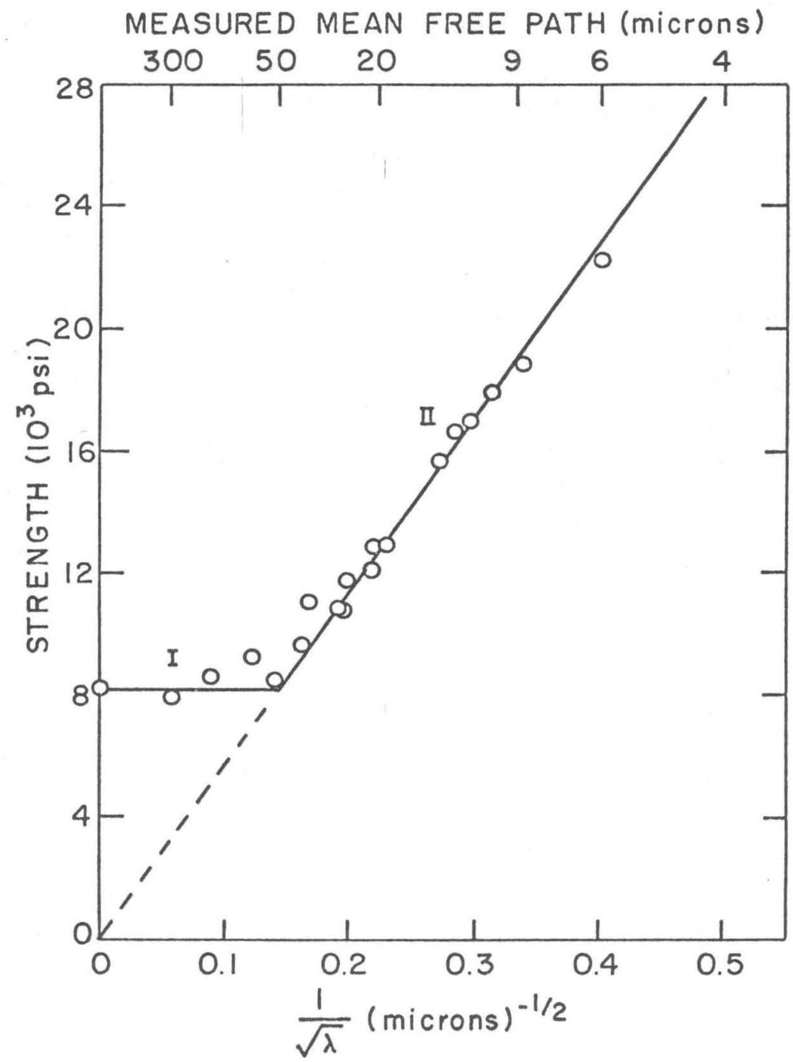

XBL 691-105

Fig. 12

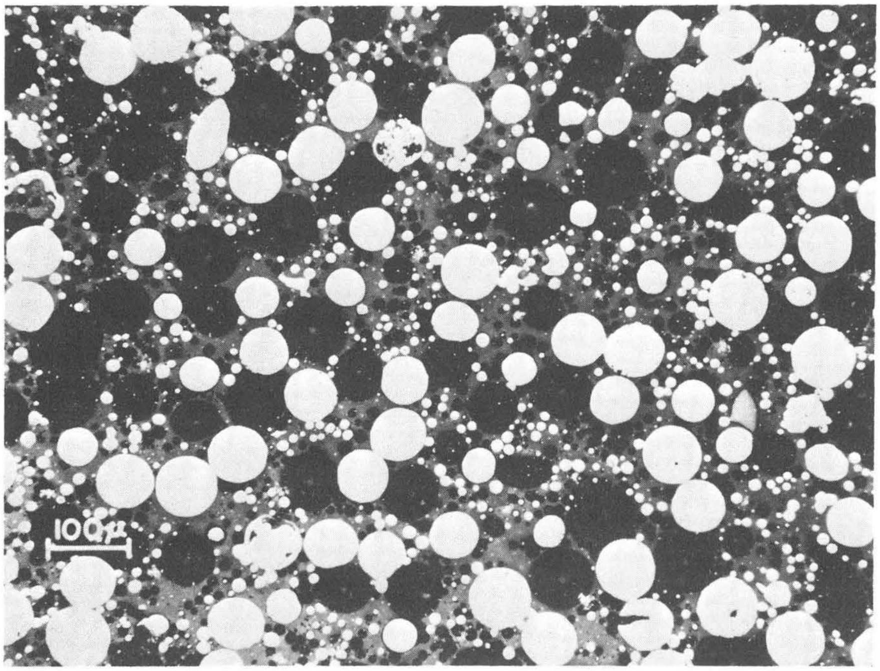

XBB 691-7

Fig. 13

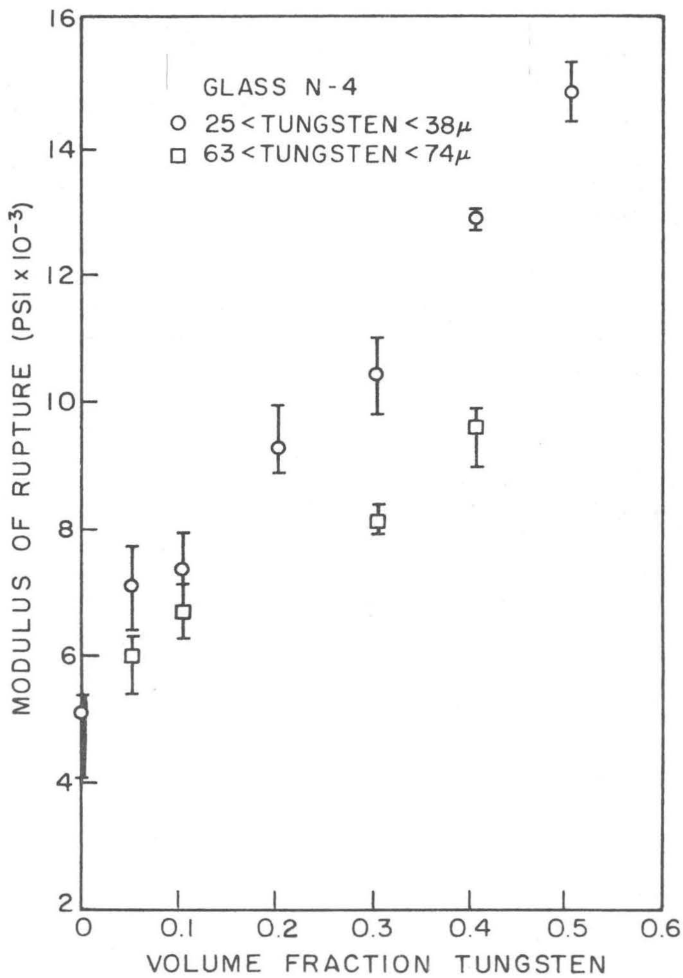

MU-31693

Fig. 14

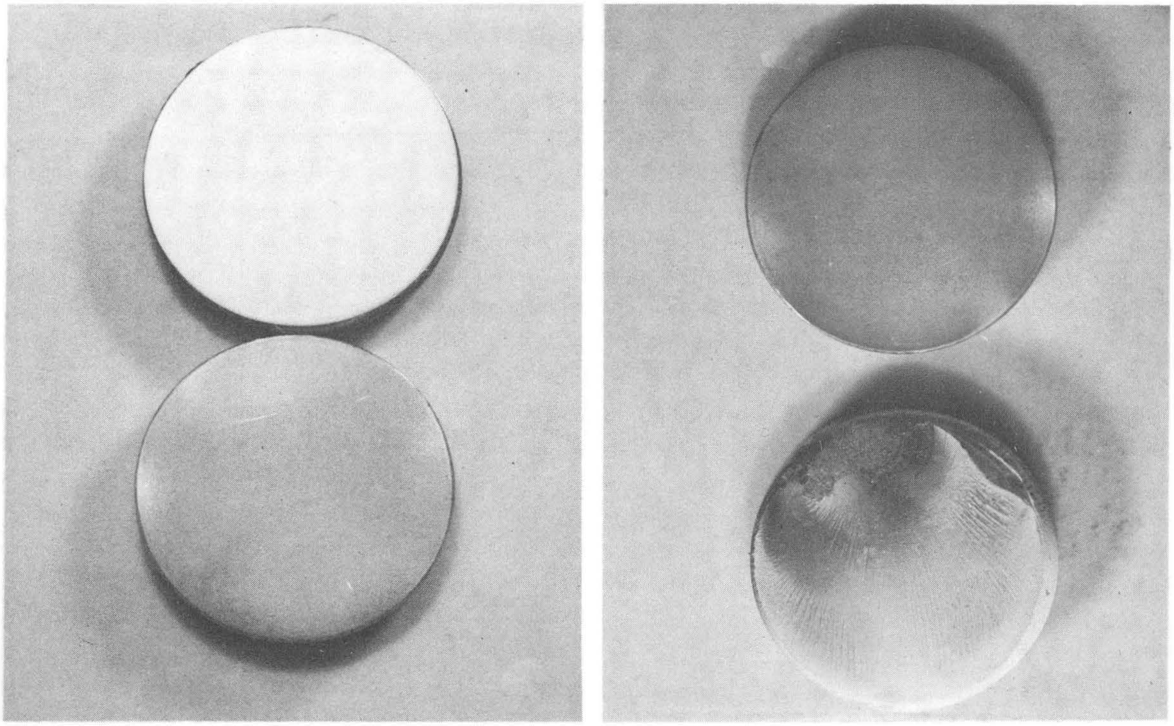

(a) (b)

IM 856

Fig. 15

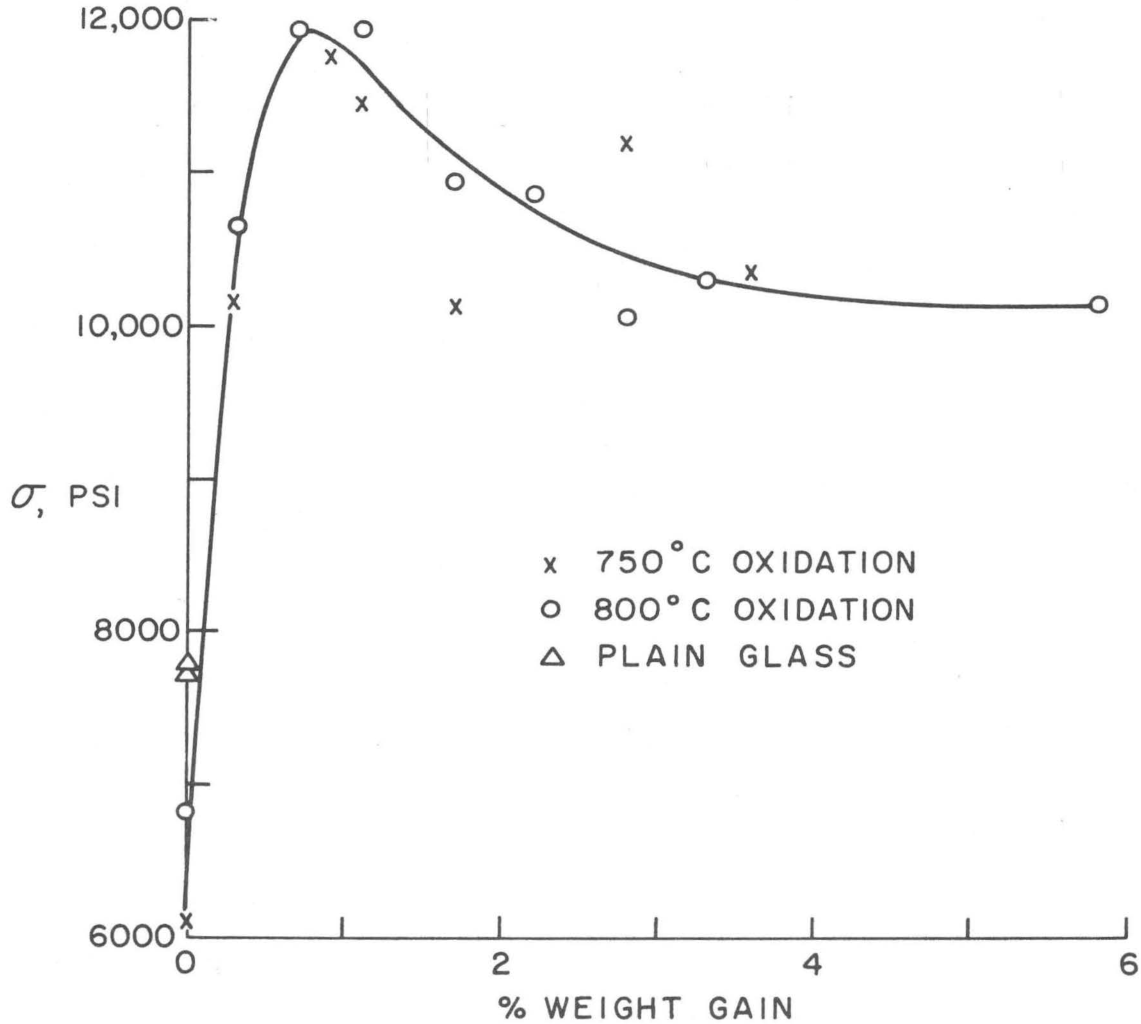

XBL 685-861

Fig. 16

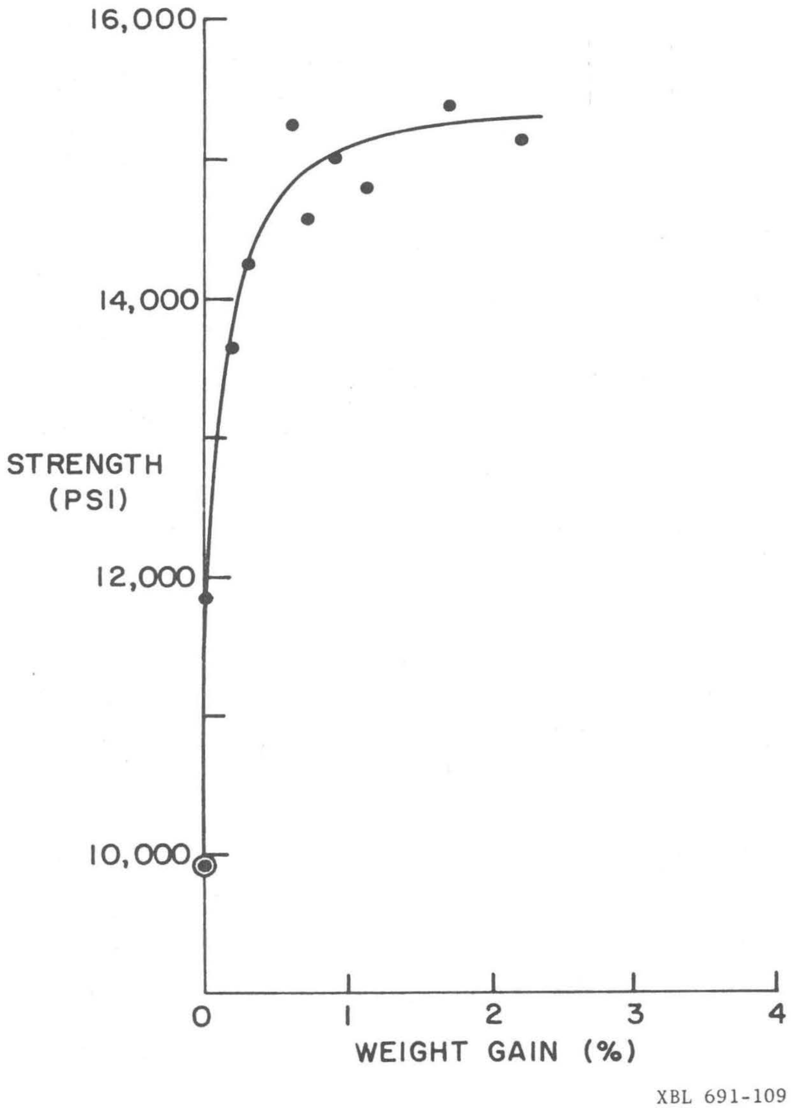
16,000
14,000
STRENGTH
(PSI)
12,000
10,000
0
1
2
3
4
WEIGHT GAIN (%)
XBL 691-109

Fig. 17

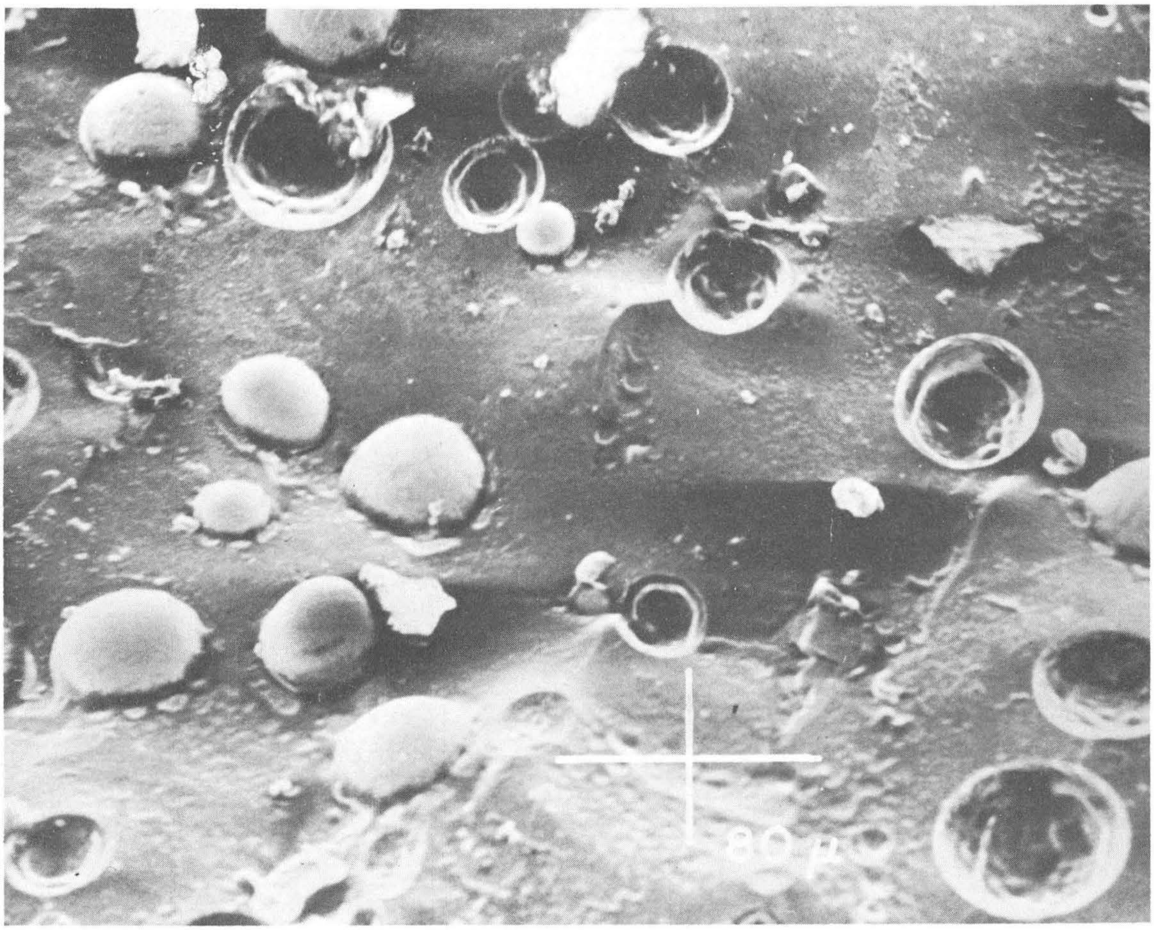

XBB 685-2984

Fig. 18

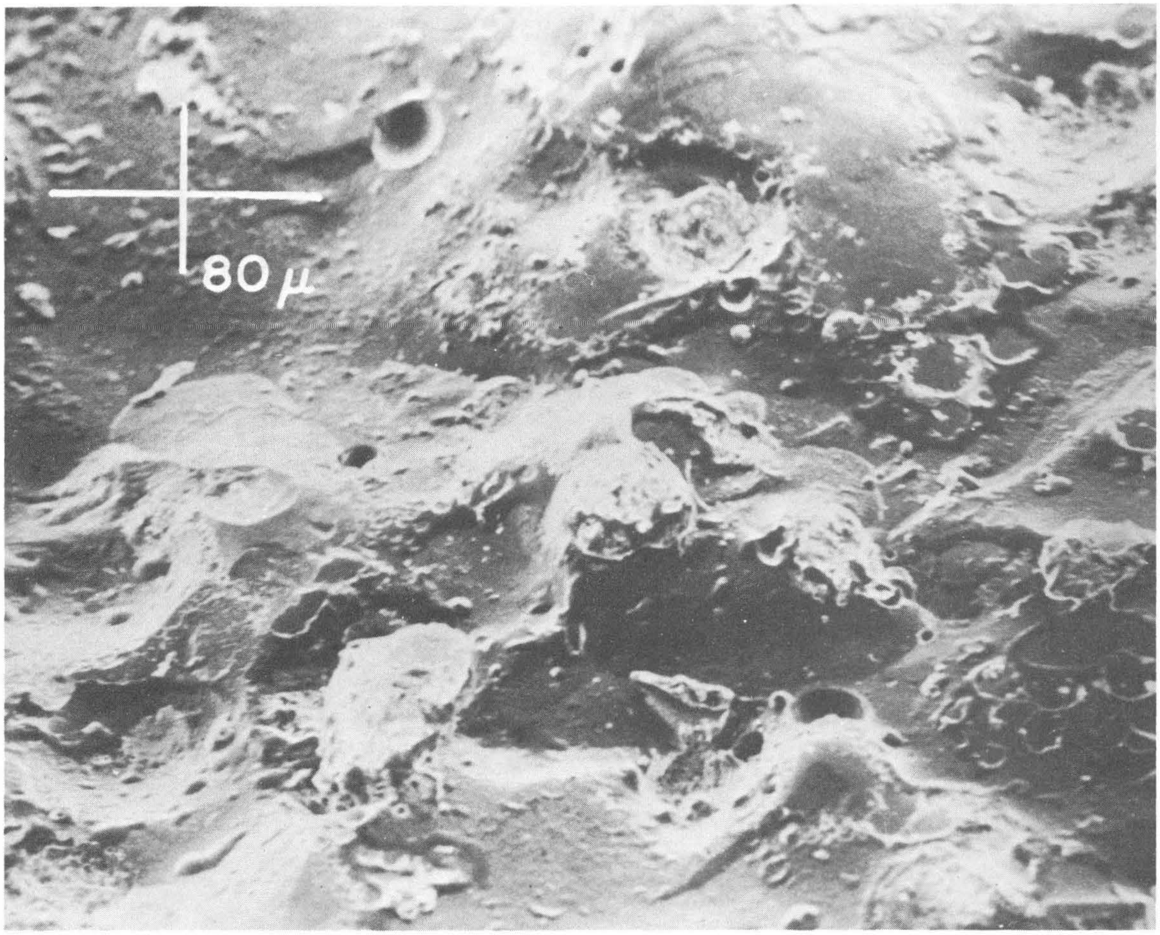

XBB 685-2983

Fig. 19

TECHNICAL INFORMATION DIVISION
LAWRENCE RADIATION LABORATORY
UNIVERSITY OF CALIFORNIA
BERKELEY, CALIFORNIA 94720